



## Synthesis and Characterization of Pure and Nitrogen Doped Titanium Oxide Nanocrystallites for Visible Light Photocatalytic Applications

R. GIRIJA<sup>1</sup>, S. STELLA MARY<sup>1,\*</sup> and G. BALAKRISHNAN<sup>2</sup>

<sup>1</sup>Department of Physics, St. Peter's Institute of Higher Education and Research, Chennai-600054, India

<sup>2</sup>Department of Physics, Bharath Institute of Science and Technology, Bharath Institute of Higher Education and Research, Chennai-600073, India

\*Corresponding author: E-mail: celstel1968@gmail.com

Received: 3 December 2020;

Accepted: 9 February 2021;

Published online: 20 March 2021;

AJC-20294

The pure and nitrogen doped titanium oxide (TiO<sub>2</sub>) nanocrystallites were synthesized using sol-gel technique. The synthesized nanoparticles were characterized to examine the microstructural, optical and photocatalytic properties. The XRD studies of pure and doped TiO<sub>2</sub> showed the formation of polycrystalline tetragonal structure with anatase phase. The crystallite sizes were calculated and found to be 17 and 15 nm for the pure and N-doped TiO<sub>2</sub>, respectively. FTIR studies indicated that the N-doped TiO<sub>2</sub> bands are stronger compared with pure TiO<sub>2</sub>, indicating the more hydroxyl groups. FESEM studies showed the uniform formation of TiO<sub>2</sub> nanocrystallites and spherical in shape with agglomeration. The photoluminescence spectra of the samples show emission peaks, indicating the band to band shift having the energy gap of 2.9 eV. The photocatalytic performance of the nanocatalyst was studied using methylene blue dye under visible light irradiation for 90 min. The photocatalytic efficiency of 66.9% and 85.8% is obtained for the pure and N-doped TiO<sub>2</sub>, respectively.

**Keywords:** Titania, Nanoparticles, Photocatalytic, X-ray diffraction, Photoluminescence, UV-visible spectroscopy.

### INTRODUCTION

Nanostructured TiO<sub>2</sub> material has attracted many scientists and researchers owing to its superior properties such as wide bandgap, high dielectric constant, high refractive index, high transparency, photoconversion efficiency, corrosion resistance, low toxicity, chemical stability and thermal stabilities with good photocatalytic activity [1,2]. Honda & Fujishima [3] discovered the photocatalytic property of TiO<sub>2</sub>. Later, it was found that the free radicals react with electrons and holes and giving the photocatalytic activity, which is based on the band-gap of the materials. The TiO<sub>2</sub> is used for many environmental and energy related applications.

Methylene blue and methylene orange dyes are highly pollutants to the environment. Discharging of these dyes to the waterbodies leads to severe health problems. Hence, various nanocatalysts are used for the photodegradation of these dyes with high efficiency [4]. Many materials such as TiO<sub>2</sub>, Fe<sub>2</sub>O<sub>3</sub>, CeO<sub>2</sub>, Al<sub>2</sub>O<sub>3</sub>, MgO and ZrO<sub>2</sub> are used as nanocatalysts for environmental related applications. Among them, TiO<sub>2</sub> is very

important photocatalytic material due to its several properties [5]. There are some drawbacks in TiO<sub>2</sub> material and hence it limits its applications. Since its bandgap is wider, the photocatalyst material can absorb energy only when its energy greater than 3.2 eV or the material will produce the electron-hole pairs under the exposure of UV radiation. The solar spectrum possess 43% visible light, 52% IR light and 5% UV light. Therefore, UV light is in smaller content and cannot be used for the practical applications [6,7]. There is a need to modify the photocatalyst with suitable bandgaps to absorb more amount of energy from the solar spectrum. Also, the higher recombination rate affects the photocatalytic activity. In addition, the weak separation of carriers leads to low photocatalytic performance. In order to overcome all the demerits, the TiO<sub>2</sub> is doped with other transitional metals, gases, rare earths and non-metals (N, B, F, Cr, V, S, P, Mn, Fe, Ni and Cu) [8-10]. It is well known that the addition of various elements into TiO<sub>2</sub>, will lead to the changes in the properties. Among them, nitrogen doping is a perfect substitute, because oxygen and nitrogen have comparable structural, chemical and other properties. Addition

of nitrogen into TiO<sub>2</sub> can decrease the energy gap and hence free radicals are produced with lesser energy leading to the usage of visible region of the electromagnetic spectrum for the photocatalytic studies. Recent reports [11,12] reported that the nitrogen addition in TiO<sub>2</sub>, decrease in the bandgap and improved photocatalytic performance. Narrowing the bandgap using nitrogen dopant, TiO<sub>2</sub> nanoparticles are expected with improved photocatalytic activity as compared to pure TiO<sub>2</sub> nanoparticles.

TiO<sub>2</sub> is known for its non-toxic, low cost, availability and stability in different environmental conditions. Because of its excellent properties, it is used in heterogeneous catalysis, photocatalysts, self cleaning windows, solar cells, gas sensors, corrosion resistant coatings, optical coatings, metal oxide field effect transistors, varistors and electro chromic devices [13-15]. TiO<sub>2</sub> exists in anatase, rutile and brookite phases. Anatase and brookite phases are the low temperature phases and thermodynamically changed to rutile phase at high temperatures. Among them, anatase phase is more important for its photocatalytic performance and adsorption of organic compounds as photocatalyst [16,17].

Therefore, synthesis of nanostructured anatase phase has gained momentum. There are many attempts to synthesize the nanocrystalline TiO<sub>2</sub> and doped TiO<sub>2</sub> for different applications [18]. Zhao *et al.* [19] prepared N-doped TiO<sub>2</sub> by sol-gel process and explored the photocatalytic activity towards methylene orange dye using visible light. Suwannaruang *et al.* [20] studied the influence of nitrogen on the structural and photocatalytic properties of TiO<sub>2</sub> catalysts calcinated at different temperatures. XRD studies showed the anatase phase in N-TiO<sub>2</sub> samples and nitrogen dopant controlled the phase transformation. The nitrogen content is noticed for 100, 300 and 400 °C. Patil *et al.* [21] reviewed the recent advances in photocatalytic efficiency and photodegradation of different contaminants in the TiO<sub>2</sub> photocatalysis for visible light.

Many techniques are used to synthesize the pure and N-doped TiO<sub>2</sub> nanoparticles. Structure and other properties are dependent on the synthesis method and the parameters used during synthesis. In the present work, the sol-gel technique was utilized due to its simple process, economical, high purity with low processing temperature for the synthesis of the pure and N-doped TiO<sub>2</sub> nanocrystallites and their structural, morphology, optical and photocatalytic properties are studied.

## EXPERIMENTAL

**Synthesis of pure and N-doped TiO<sub>2</sub>:** Sol-gel technique is employed to synthesize the pure and nitrogen-doped TiO<sub>2</sub> nanocrystallites. In this method, 20 mL of titanium isopropoxide precursor is dissolved in solvent consist of 45 mL ethanol, 5 mL of deionized water and 2 mL of Triton X-100 was added. The solution is stirred for 1 h at 60 °C and then temperature was raised to 110 °C in oven for 1 h. The obtained white material was centrifuged for three times using distilled water and ethanol. The material was dried at 110 °C for 6 h and calcinated at 500 °C for 2 h. Urea (2 g), as nitrogen precursor, was mixed with titanium isopropoxide solution for the synthesis of N-doped TiO<sub>2</sub> particles.

**Characterization:** X-ray diffractometer (XRD) was employed to analyze the structural property of the samples (Rigaku with CuK $\alpha$  radiation). FTIR spectrometer (Thermo Nicolet Model: 6700) was used to analyze the presence of chemical bonds in the prepared nanocrystallites in the range 4000-400 cm<sup>-1</sup>. The optical properties were investigated using the spectrofluorimeter (Model: FLUOROLOG-FL3-11; Jobin Yvon) with 350 nm excitation wavelength. The surface topography and compositions were analyzed by field emission scanning electron microscope (FESEM) (Zeiss-Microscopy Ltd.). The photocatalytic performance of the nanocatalysts was studied using the photoreactor (HEBER, MODELHVAR-MP400) with visible light (150 W) irradiation. The reflectance of the nanoparticles was analyzed using UV-VIS-NIR spectrophotometer (Varian Model: 5000).

**Photocatalytic activity:** The photocatalytic performance was investigated for the pure and N-doped TiO<sub>2</sub> nanoparticles in an aqueous solution irradiated with visible light and methylene blue dye used as a model pollutant. Around 100 mg of pure and doped nanocrystallites were dispersed in 100 mL of methylene blue dye solutions (10 ppm) using ultrasonication. The catalytic performance was analyzed after stirring the solution for 30 min at dark condition to attain the equilibrium condition between the catalyst and model pollutant. The solution is taken at regular intervals to analyze the absorbance of the samples. The photocatalytic degree of discolouration of methylene blue dye was determined using 100 mL of dye aqueous solution with 10 ppm initial concentration and this value was higher than the wastewaters concentration, discharged from textile dye factories.

## RESULTS AND DISCUSSION

**XRD studies:** XRD pattern of the pure and nitrogen-doped TiO<sub>2</sub> nanocrystallites prepared using sol-gel method is shown in Fig. 1. The XRD pattern shows the peaks at angles 25.27°, 37.86°, 48.1°, 53.9°, 55.1°, 62.7°, 68.9°, 70.25°, 75.0° and 82.8°, representing (101), (004), (200), (105), (211), (204), (116), (220) and (215) reflections belong to tetragonal structure of TiO<sub>2</sub> with anatase phase [JCPDS card no. 21-1272]. The weak peak at an angle 30.77° indicates the brookite phase of TiO<sub>2</sub> with (121) orientation [JCPDS card No. 29-1360]. The Scherrer's formula was applied to calculate the crystallite size from A (101) peak of the samples:

$$D = \frac{K\lambda}{\beta \cos \theta}$$

where K is the Scherrer constant (0.9),  $\lambda$  is the wavelength of X-rays (1.5418 Å),  $\beta$  is the full-width at half maximum (FWHM) and  $\theta$  is the diffraction angle. The crystallite size of the pure TiO<sub>2</sub> was found to be 17 nm.

N-doped TiO<sub>2</sub> sample exhibited the peaks at angles 25.3°, 30.9°, 37.8°, 48.2°, 53.9°, 55.0°, 62.8°, 68.8°, 70.3°, 75.1°, 82.7° indicating the (101), (004), (200), (105), (211), (204), (116), (220), (215) and reflections of polycrystalline anatase phase of tetragonal structure. The diffraction angle was slightly shifted to the higher angle side for the N-doped sample, indicating the stress. The intensity of Brookite (121) is relatively higher in the pure TiO<sub>2</sub> sample compared to N-doped sample. The

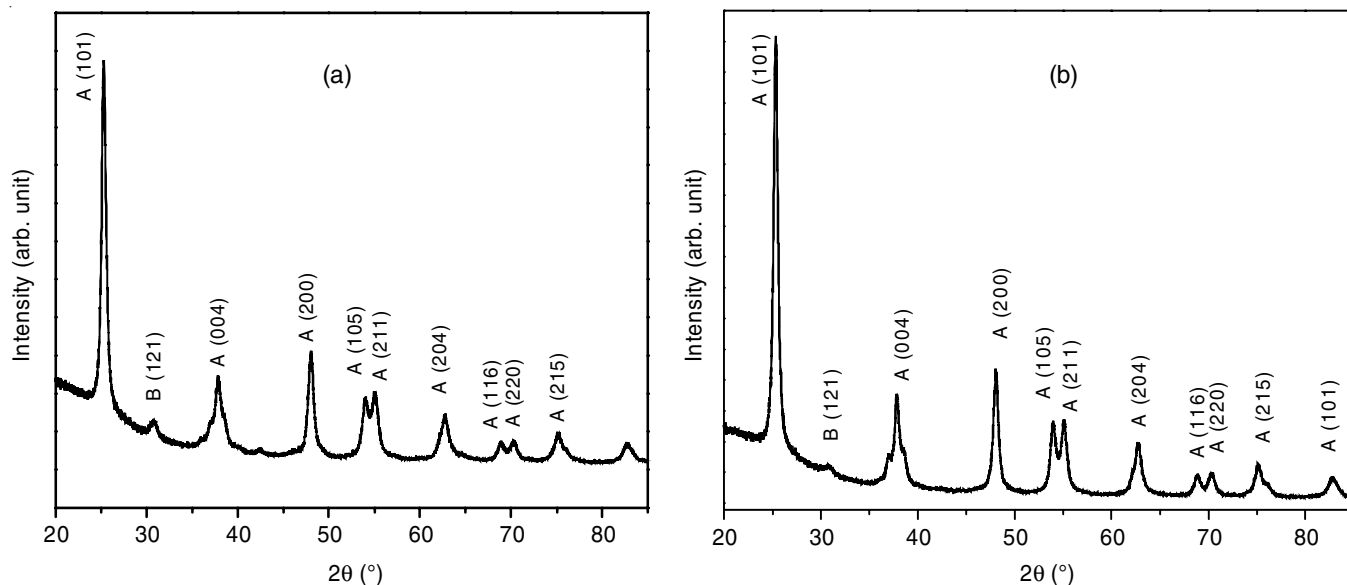


Fig. 1. XRD pattern of pure TiO<sub>2</sub> Nanoparticles (a) and N-doped TiO<sub>2</sub> nanoparticles (b)

high intense A (101) peak is used for the calculation of crystallite sizes in the N-doped sample and found to be 15 nm. In both the samples, percentage of the anatase phase much greater than the brookite phase as it is known from the intensity of these two phases [21,22]. Sathiyar *et al.* [23] synthesized pure TiO<sub>2</sub> nanoparticles using titanium tetrachloride as precursor and the XRD studies indicated the anatase and brookite phases of TiO<sub>2</sub>. Zhao *et al.* [24] showed that the anatase, rutile and brookite phases are dependent on the crystallite size.

**FTIR studies:** FTIR spectrum of the pure and N-doped TiO<sub>2</sub> nanoparticles is shown in Fig. 2. The pure TiO<sub>2</sub> shows the peaks at 2845, 2915, 2145, 1970, 1730, 1450 cm<sup>-1</sup>, whereas N-doped TiO<sub>2</sub> exhibited the peaks at 2140, 1725, 1650, 1440, 1270, 970 cm<sup>-1</sup>. The peak at ~ 3500-3000 cm<sup>-1</sup> is due to O-H stretching vibration present in the sample. The peak at ~1650 cm<sup>-1</sup> is attributed to the H-O-H vibrational bond on the surface. The peaks in the 970-400 cm<sup>-1</sup> wave number range is assigned to Ti-O-Ti stretching vibration bonds. The two absorption

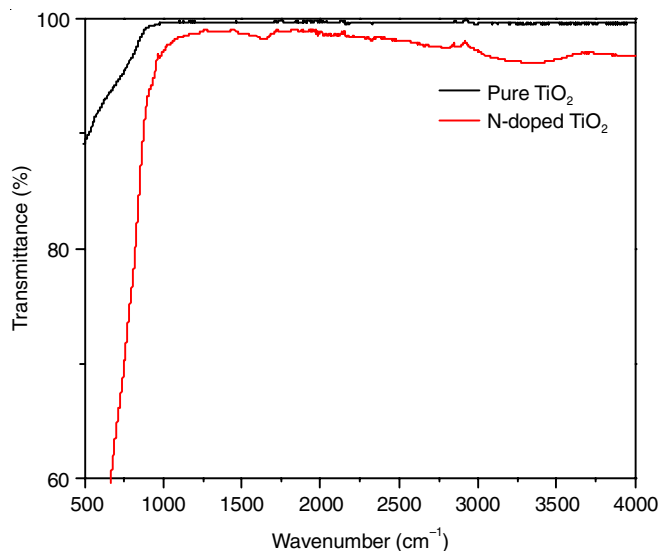


Fig. 2. FTIR spectra of the pure and N-doped TiO<sub>2</sub> nanoparticles

bands (~3500 and ~1600 cm<sup>-1</sup>) intensity in the doped TiO<sub>2</sub> is stronger compared with pure TiO<sub>2</sub>, indicating more surface adsorbed water and O-H groups, which plays a vital function in photocatalytic activity [23].

**Surface morphology:** Fig. 3 shows the surface morphology of pure and N-doped TiO<sub>2</sub> nanoparticles. The FE-SEM images confirm the arrangement of the nanocrystallites by different magnifications (10 KX and 60 KX). These images showed the TiO<sub>2</sub> nanoparticles uniform in size, dense structure with agglomeration. It is also observed that the crystallite size of doped TiO<sub>2</sub> nanocrystallites are larger as compared to pure TiO<sub>2</sub> nanoparticles, porous in nature and the result is in good agreement with other reported studies [23].

**Photoluminescence studies:** Photoluminescence spectra of the pure and N-doped TiO<sub>2</sub> nanoparticles are shown in Fig. 4. Photoluminescence spectrum of pure TiO<sub>2</sub> nanoparticles showed two emission peaks at 395 and 452 nm. The N-doped TiO<sub>2</sub> nanoparticles also indicating two peaks at 385 and 452 nm. The peak at 395 nm is due to the oxygen vacancies in the samples. The emission at 452 nm represents the bandgap of about (2.74 eV). It was observed that the intensity in the doped TiO<sub>2</sub> is less compared to pure TiO<sub>2</sub> sample, due to the electron-hole pairs recombination suppression, which makes the catalyst photoactive. Rajamanickam *et al.* [25] prepared pure TiO<sub>2</sub> and TiO<sub>2</sub> activated carbon composite by sol-gel process and the photoluminescence studies showed the emission about 450 nm. The present result is in concurrence with the other reported results.

**Optical studies:** Fig. 5 shows the DRS spectra of the pure and nitrogen-doped TiO<sub>2</sub> nanoparticles indicating a sharp reflectance of materials near the visible region. The absorption is slightly shifted to higher wavelength region for the N-doped TiO<sub>2</sub> nanoparticles. The optical bandgap is calculated from the reflectance using the Kubelka-Munk (K-M) function as follows:

$$F(R) = \frac{(1-R)^2}{2R}$$

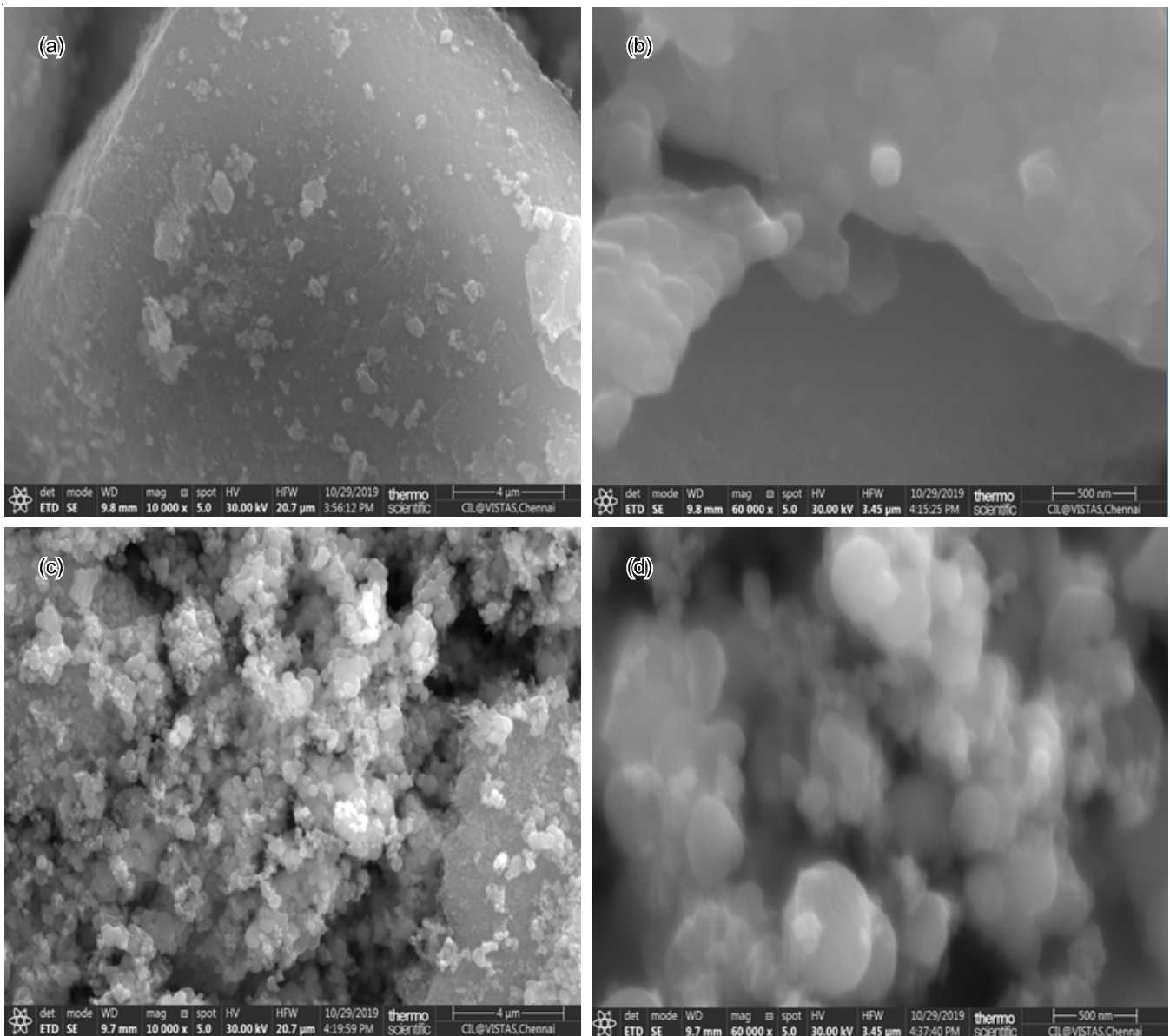


Fig. 3. FESEM image of Pure  $\text{TiO}_2$  with 10 KX and 60 KX (a-b) and N-doped  $\text{TiO}_2$  with 10 KX and 60 KX (c-d)

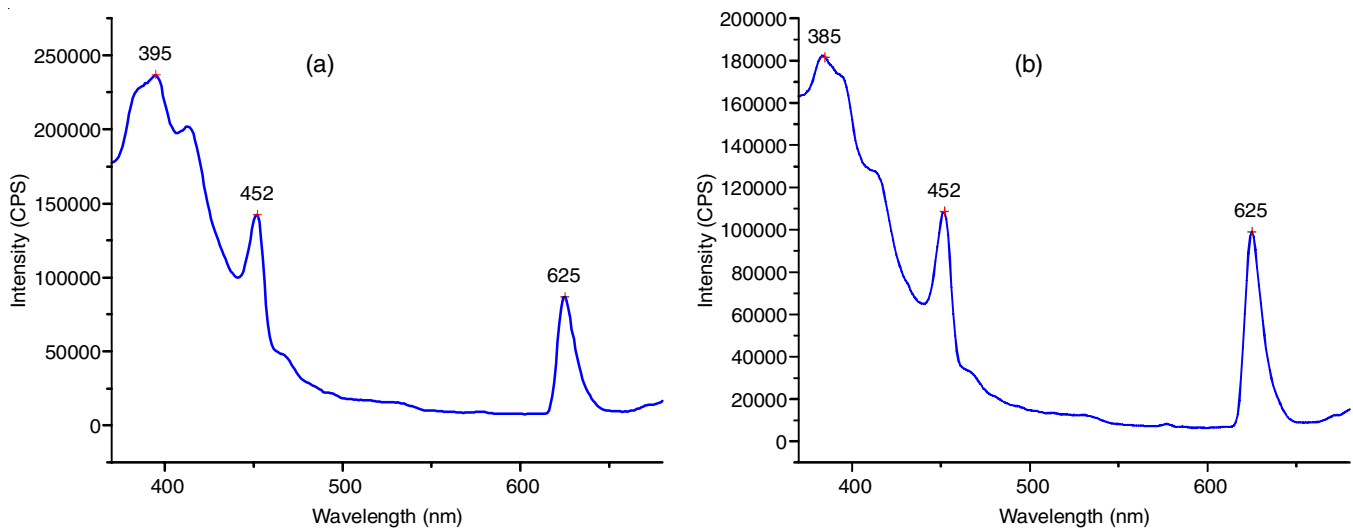


Fig. 4. Photoluminescence spectra of pure  $\text{TiO}_2$  nanoparticles (a); and N-doped  $\text{TiO}_2$  nanoparticles (b)

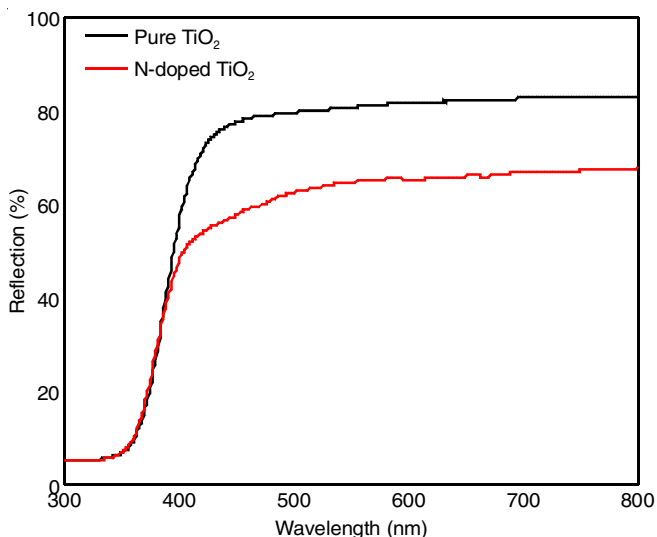


Fig. 5. UV-visible diffuse reflection spectra of pure and N-doped TiO<sub>2</sub> nanoparticles

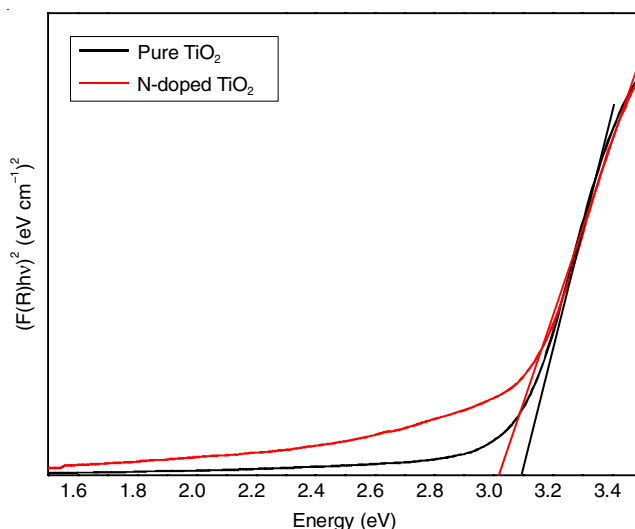


Fig. 6. Kubelka-Munk plot of pure and doped TiO<sub>2</sub> nanoparticles

where R is the reflectance of the sample. The wavelength is converted to energy and plotting the graph  $[F(R)h\nu]^2$  vs.  $h\nu$  and the tangent is drawn to the linear region and the intercept at X-axis denote the bandgap of the material (Fig. 6). The bandgap of the samples was calculated and found to be 3.1 and 3.0 eV for pure and doped TiO<sub>2</sub>, respectively. The inclusion of dopant atoms in the TiO<sub>2</sub> lattice is proved by the decrease of bandgap from 3.1 eV (pure TiO<sub>2</sub>) to 3.0 eV (N-TiO<sub>2</sub>). For N-doped sample, reflection is less as compared to pure TiO<sub>2</sub>, indicating the loss of nitrogen atoms at higher annealed temperatures [9]. Nitrogen doping decreased the bandgap of TiO<sub>2</sub> due to the trapping level between valence and conduction band induced by N-doping [10,23,25]. It is well known that the  $E_g$  is an significant parameter to evaluate the photocatalytic property and the materials yield excellent performance as the materials with lowest bandgap. In the present work, one could observed from the DRS spectra that the bandgap of N-doped TiO<sub>2</sub> is not reduced much. This is due to the loss of nitrogen in

TiO<sub>2</sub> during calcination process (500 °C), resulting the low nitrogen in the TiO<sub>2</sub> structure and hence there is minimum variation in the bandgap [20].

**Photocatalytic studies:** Photocatalytic performance of the pure and doped TiO<sub>2</sub> particles is studied using methylene blue dye with visible light exposure. Fig. 7 shows the methylene blue dye degradation as a function of time. The experiments were performed at room temperature and suspension was stirred for 30 min at dark condition to reach equilibrium between the model pollutant and catalyst. The suspension was irradiated under visible light (Haber Model, India) with 150 W power. All the photocatalytic activities were carried out with constant stirring rate. The suspension solution is aerated continuously to provide oxygen during photocatalytic experiments. A fixed quantity (3 mL) of methylene blue suspension was taken at every 15 min during the irradiation period and absorbance of the solution was measured. The process of discoloring was monitored using spectrophotometer in the 400-700 nm wavelength range. The variation in the intensity of absorbance was

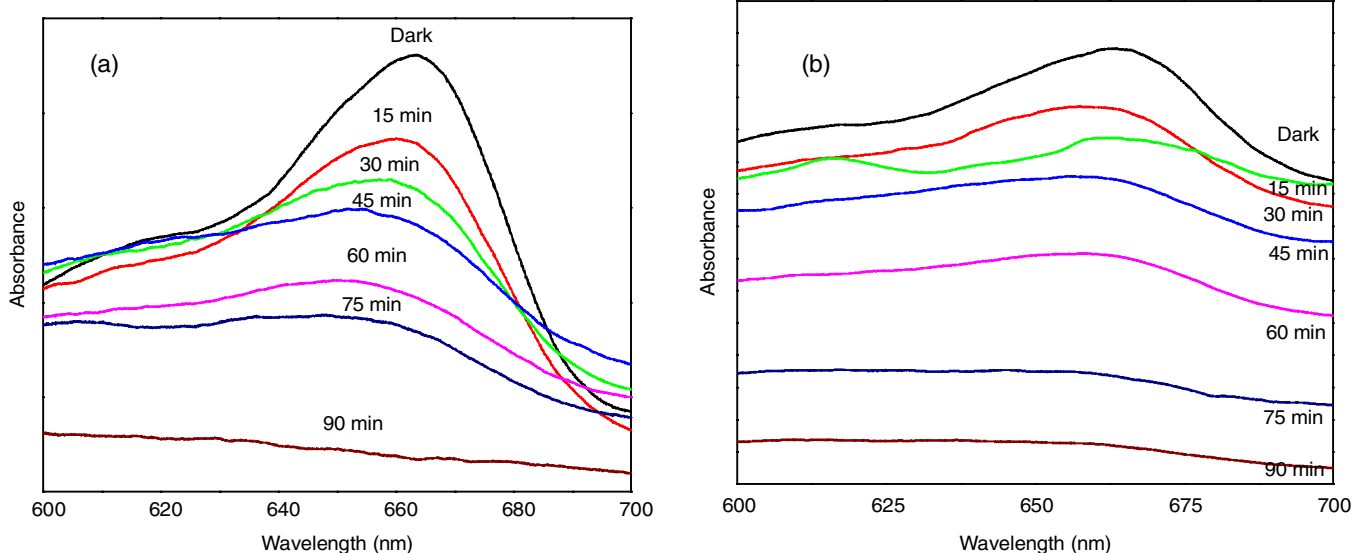


Fig. 7. Photodegradation studies of methylene blue dye using pure TiO<sub>2</sub> (a) and N-doped TiO<sub>2</sub> as catalyst (b)

decreased with increasing time. The methylene blue degradation efficiency (%) was calculated as below:

$$\frac{A_0 - A_t}{A_0} \times 100$$

where  $A_0$  and  $A_t$  are the absorbance values at  $t = 0$  and  $t = 15$  min at 664 nm wavelength (maximum absorbance of methylene blue dye).

It was observed that the absorption decreased with increasing irradiation time. Electron-hole pairs are generated in  $\text{TiO}_2$ , due to irradiation of light and the carriers move to the surface, where it reacts with adsorbed water and oxygen and radical species are produced. The adsorbed organic molecules cause decomposition into  $\text{CO}_2$  and  $\text{H}_2\text{O}$ . This process can be employed ranging from purification of wastewater to self-cleaning coatings [26]. It was observed that the maximum absorption peak is shifted slightly to the lower wavelength side and this is due to the intermediates formation during the photocatalytic activity [27]. Narrowing the bandgap of nitrogen doped  $\text{TiO}_2$  showed the improved catalytic properties [10]. The band gap reduction was due to the creation of intra bands from the N-dopant, resulting in the energy gap reduction and supporting the visible light absorption [16]. The photocatalytic activities of the pure  $\text{TiO}_2$  catalyst is compared with N-doped  $\text{TiO}_2$  catalyst. The pure  $\text{TiO}_2$  catalyst exhibits the photocatalytic efficiency of 66.9%, while the N-doped  $\text{TiO}_2$  is 85.8% in 120 min. The reduced bandgap due to the doping of nitrogen increased the absorption of visible light, hence increasing the photocatalytic performance in the doped  $\text{TiO}_2$  as compared with pure  $\text{TiO}_2$ .

## Conclusion

Pure and nitrogen doped  $\text{TiO}_2$  nanostructured materials were prepared using the sol-gel process. The microstructure, optical properties and photocatalytic behaviour of the nanocrystallites were also investigated. The XRD results revealed the tetragonal structure of anatase phase with small quantity of brookite phase in the samples. The FESEM studies showed the surface morphology of pure and doped  $\text{TiO}_2$  samples, indicating formation of nanocrystallites with agglomeration. The photoluminescence spectroscopy studies revealed the bandgap of bandgap of 2.74 eV. The DRS studies indicated the bandgap of 3.1 and 3.0 eV for the pure and doped  $\text{TiO}_2$ , respectively. Photocatalytic studies revealed the photocatalytic efficiency of 66.9% for the pure  $\text{TiO}_2$ , whereas it is 85.8% for the N-doped  $\text{TiO}_2$  for methylene blue dye. Since, the pure and doped samples showed the higher photocatalytic efficiency using visible light irradiation and can be used in wastewaters treatment and other environmental related applications.

## CONFLICT OF INTEREST

The authors declare that there is no conflict of interests regarding the publication of this article.

## REFERENCES

- P.V. Kamat, *J. Phys. Chem. C*, **116**, 11849 (2012); <https://doi.org/10.1021/jp305026h>
- M. Ge, C. Cao, J. Huang, S. Li, Z. Chen, K.-Q. Zhang, S.S. Al-Deyab and Y. Lai, *J. Mater. Chem. A*, **4**, 6772 (2016); <https://doi.org/10.1039/C5TA09323F>
- E. Katouezadeh, S.M. Zebarjad and K. Janghorban, *J. Mater. Res. Technol.*, **8**, 541 (2019); <https://doi.org/10.1016/j.jmrt.2018.04.013>
- G. Balakrishnan, R. Velavan, K.M. Batoo and E.H. Raslan, *Results Phys.*, **16**, 103013 (2020); <https://doi.org/10.1016/j.rinp.2020.103013>
- R. Bashiri, N.M. Mohamed and C.F. Kait, Recent Applications in Sol-Gel Synthesis, In: Advancement of Sol-Gel Prepared  $\text{TiO}_2$  Photocatalyst, Intech Publishers, (2017).
- F. Huang, A. Yan and H. Zhao, Influences of Doping on Photocatalytic Properties of  $\text{TiO}_2$  Photocatalyst, In: Semiconductor Photocatalysis-Materials, Mechanisms and Applications, Intech Publishers, Chap. 2, pp 31-80 (2016).
- S.D. Delekar, H.M. Yadav, S.N. Achary, S.S. Meena and S.H. Pawar, *Appl. Surf. Sci.*, **263**, 536 (2012); <https://doi.org/10.1016/j.apsusc.2012.09.102>
- L. Ji, Y. Zhang, S. Miao, M. Gong and X. Liu, *Carbon*, **125**, 544 (2017); <https://doi.org/10.1016/j.carbon.2017.09.094>
- J. Marques, T.D. Gomes, M.A. Forte, R.F. Silva and C.J. Tavares, *Catal. Today*, **326**, 36 (2019); <https://doi.org/10.1016/j.cattod.2018.09.002>
- A. Eshaghi and H. Moradi, *Adv. Powder Technol.*, **29**, 1879 (2018); <https://doi.org/10.1016/j.apt.2018.04.026>
- N. Erdogan, A. Bouziani, J. Park, M. Micusik, S.Y. Kim, E. Majkova, M. Omastova and A. Ozturk, *J. Photochem. Photobiol. Chem.*, **377**, 92 (2019); <https://doi.org/10.1016/j.jphotochem.2019.03.047>
- V. Etacheri, C. Di Valentin, J. Schneider, D. Bahnemann and S.C. Pillai, *J. Photochem. Photobiol. Photochem. Rev.*, **25**, 1 (2015); <https://doi.org/10.1016/j.jphotochemrev.2015.08.003>
- X.G. Zhao and L.Q. Huang, *Ceramics Int.*, **43**, 3975 (2017); <https://doi.org/10.1016/j.ceramint.2016.11.083>
- G. Balakrishnan, S. Manavalan, R. Venkatesh Babu and J.I. Song, Effect of Substrate Temperature on Microstructure and Properties of Nanocrystalline Titania Thin Films Prepared by Pulsed Laser Deposition, *Nanosystems: Physics, Chemistry, Mathematics*, **7**, 621 (2016).
- G. Balakrishnan, V.R. Bandi, S.M. Rajeswari, N. Balamurugan, R.V. Babu and J.I. Song, *Mater. Res. Bull.*, **48**, 4901 (2013); <https://doi.org/10.1016/j.materresbull.2013.07.009>
- T. Tachikawa, S. Yamashita and T. Majima, *J. Am. Chem. Soc.*, **133**, 7197 (2011); <https://doi.org/10.1021/ja201415j>
- R. Abazari, A.R. Mahjoub and S. Sanati, *RSC Adv.*, **4**, 56406 (2014); <https://doi.org/10.1039/C4RA10018B>
- J. Ananpattarachai, P. Kajitvichyanukul and S. Seraphin, *J. Hazard. Mater.*, **168**, 253 (2009); <https://doi.org/10.1016/j.jhazmat.2009.02.036>
- W. Zhao, S. Liu, S. Zhang, R. Wang and K. Wang, *Catal. Today*, **337**, 37 (2019); <https://doi.org/10.1016/j.cattod.2019.04.024>
- T. Suwannaruang, N. Chanlek, K. Kamonsuangkasem, P. Kidkhunthod, P. Chirawatkul, C. Saiyasombat and K. Wantala, *Mater. Res. Bull.*, **105**, 265 (2018); <https://doi.org/10.1016/j.materresbull.2018.05.010>
- B.S. Patil, S.B. Patil, N. Ganganagappa, K.R. Reddy, A.V. Raghu and Ch. Venkata Reddy, *Int. J. Hydrogen Energy*, **45**, 7764 (2020); <https://doi.org/10.1016/j.ijhydene.2019.07.241>
- S.M. Reda, M.A. Khairy and M.A. Mousa, *Arab. J. Chem.*, **13**, 86 (2020); <https://doi.org/10.1016/j.arabjc.2017.02.002>
- K. Sathiyar, R. Bar-Ziv, O. Mendelson and T. Zidki, *Mater. Res. Bull.*, **126**, 110842 (2020); <https://doi.org/10.1016/j.materresbull.2020.110842>
- A. Sanchez-Martinez, O. Ceballos-Sanchez, C. Koop-Santa and R. Edgar, *Ceram. Int.*, **44**, 5273 (2017); <https://doi.org/10.1016/j.ceramint.2017.12.140>
- D. Rajamanickam and M. Shanthi, *Spectrochim. Acta A Mol. Biomol. Spectrosc.*, **128**, 100 (2014); <https://doi.org/10.1016/j.saa.2014.02.126>
- L. Zhao, Y. Xie, Q. Lin, R. Zheng and Y. Diao, *Funct. Mater. Lett.*, **12**, 1950045 (2019); <https://doi.org/10.1142/S1793604719500450>
- T. Liu, L. Wang, X. Lu, J. Fan, X. Cai, B. Gao, R. Miao, J. Wang and Y. Lv, *RSC Adv.*, **7**, 12292 (2017); <https://doi.org/10.1039/C7RA00199A>